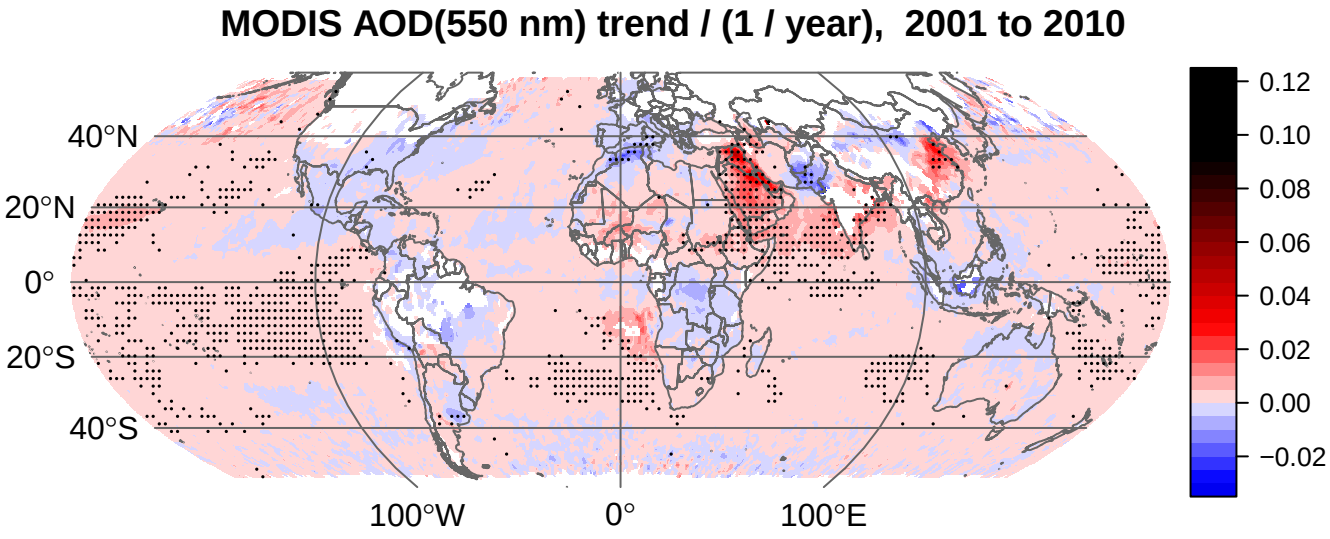

Figure S1. Same as Fig. 1 but for the ten year time period January 2001 to December 2010.

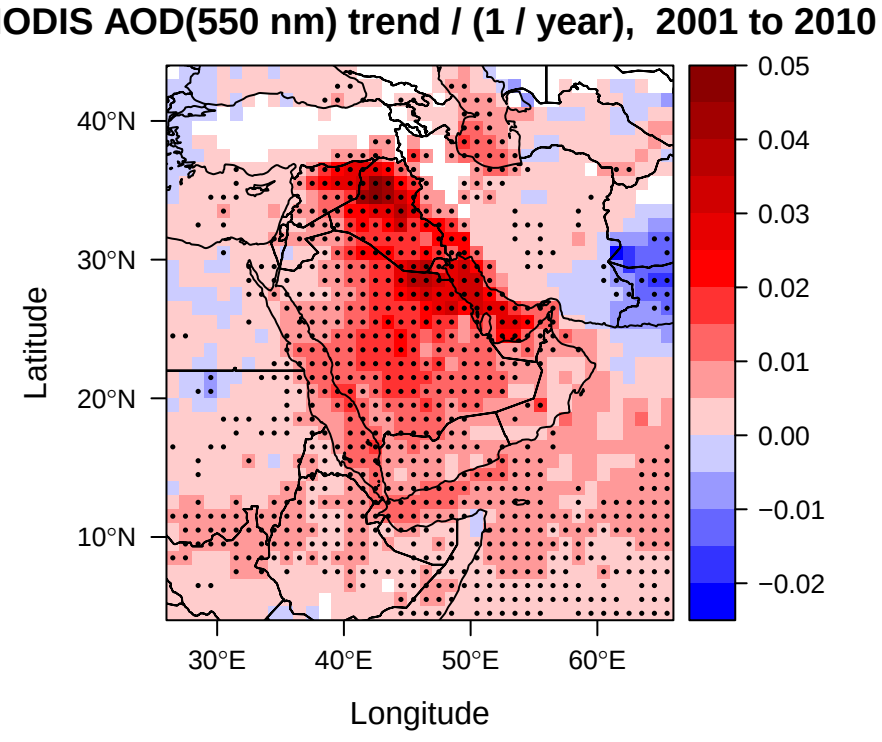

Figure S2. Same as Fig. 2 but for the ten year time period January 2001 to December 2010.

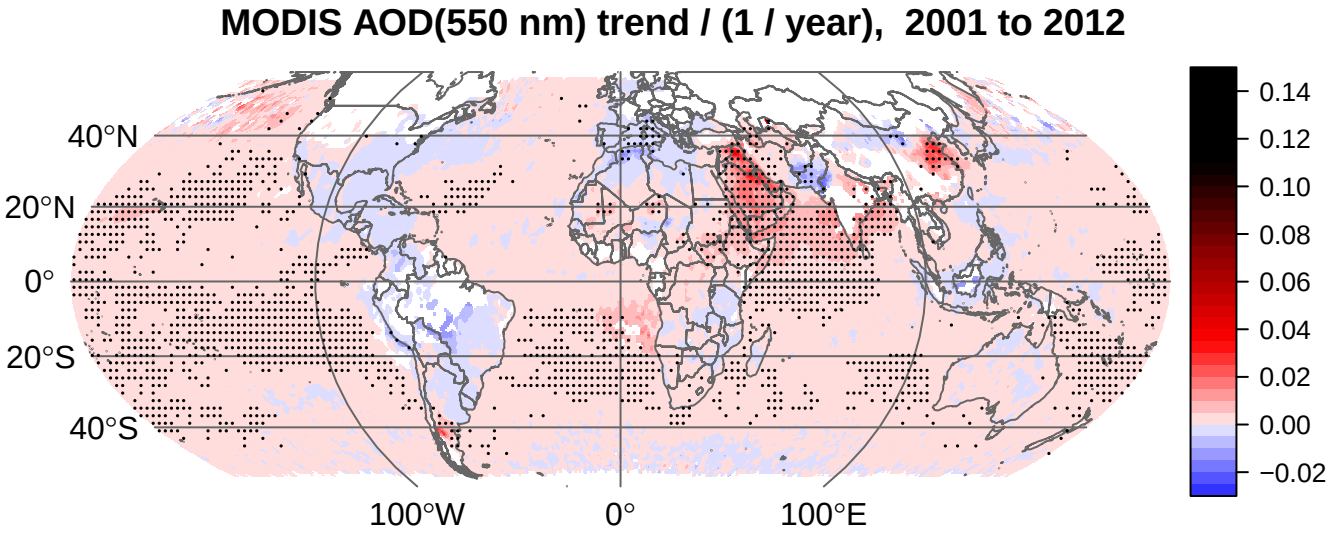

Figure S3. Same as Fig. 1 but for the twelve year time period January 2001 to December 2012.

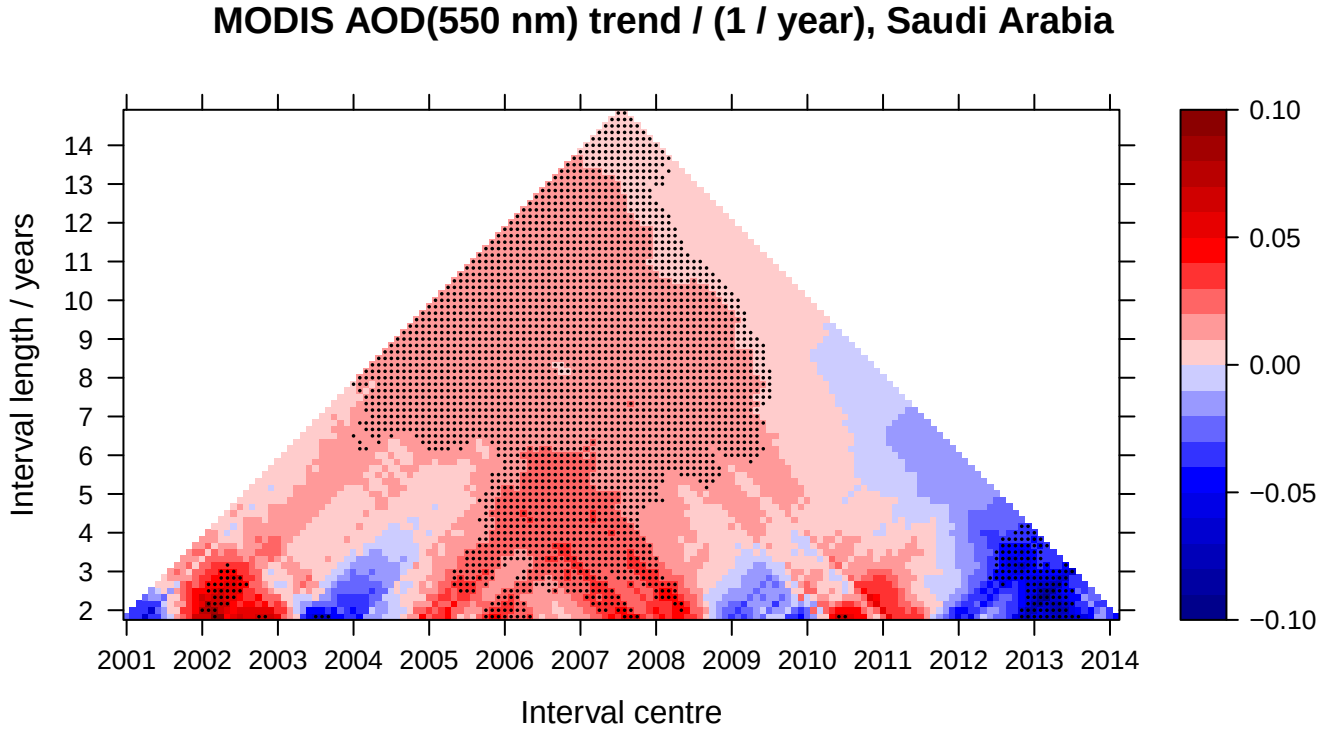

Figure S4. Trend triangle plot for the average Saudi Arabian 550 nm AOD. The abscissa depicts the centre of the time interval considered for the trend analysis using linear regression, the ordinate shows the length of the interval. Time intervals with significant trend (p value $<$ 0.01) are marked with a dot. Deseasonalisation and trend analysis is performed as for Fig. 3.

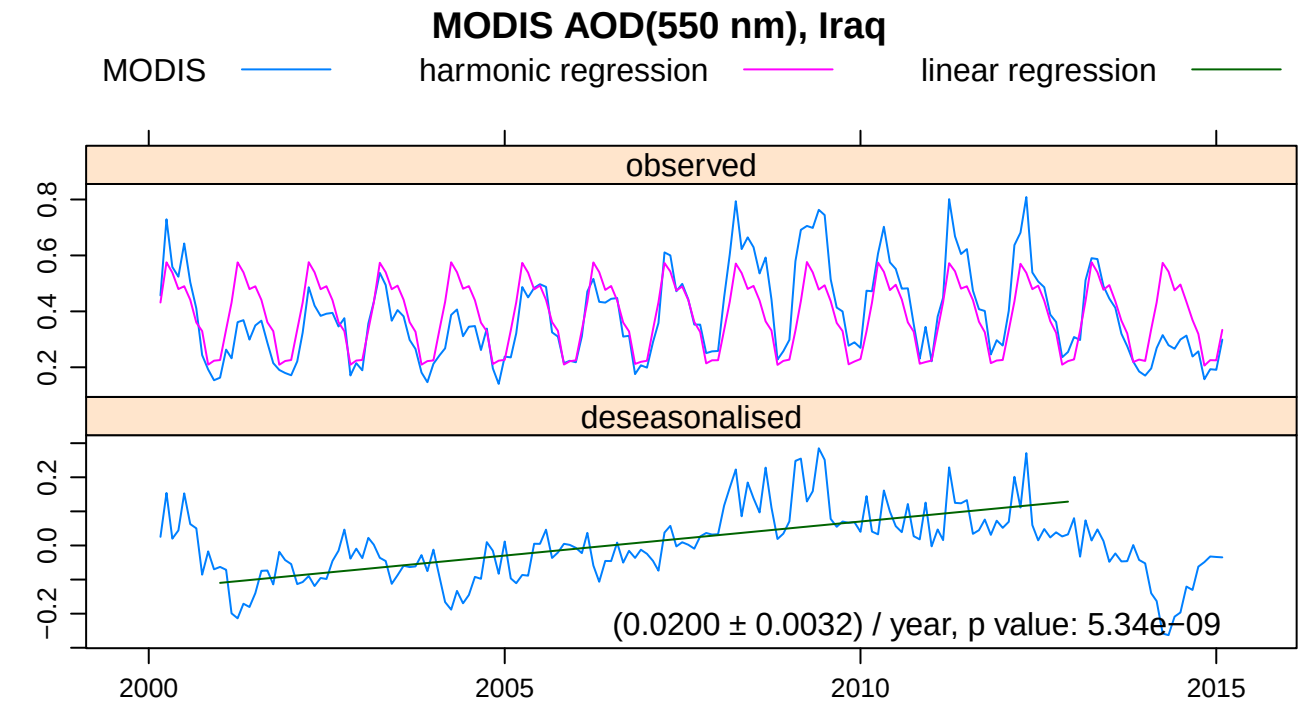

Figure S5. Same as Fig. 3, but for Iraq.

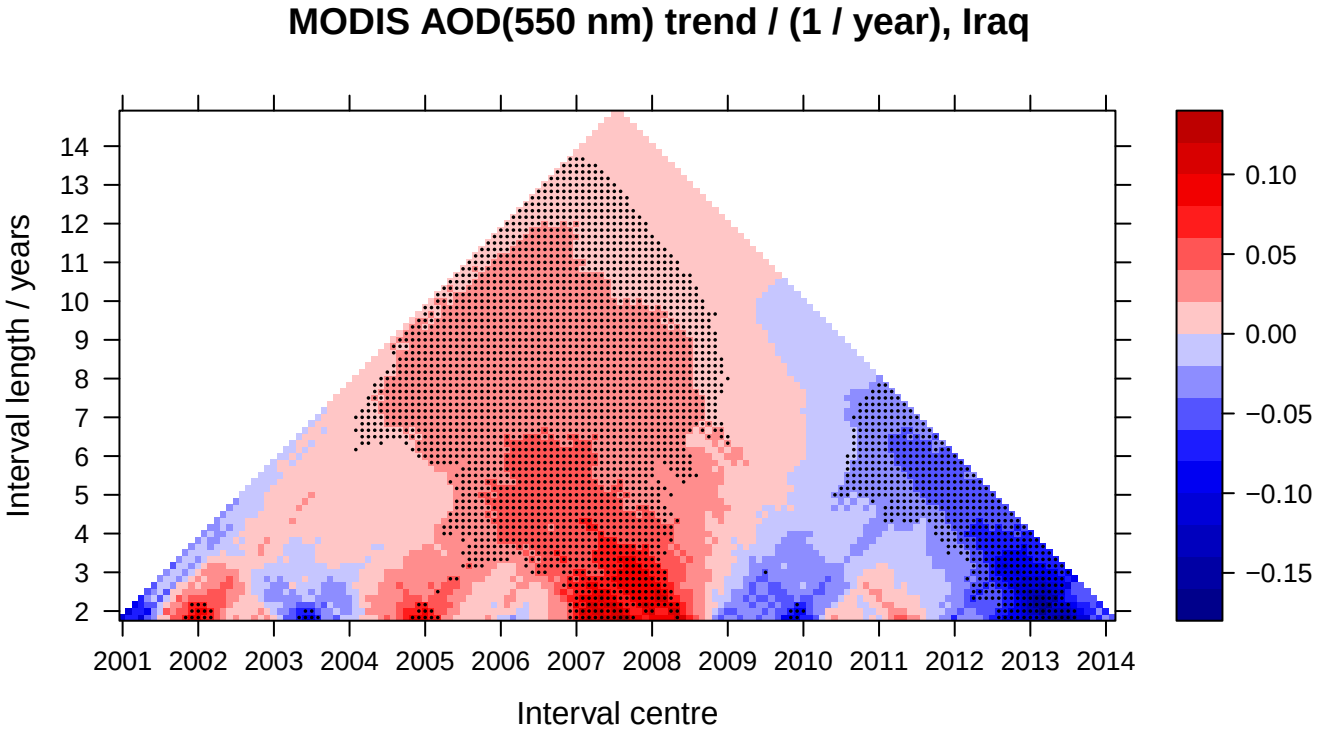

Figure S6. Same as Fig. S4, but for Iraq.

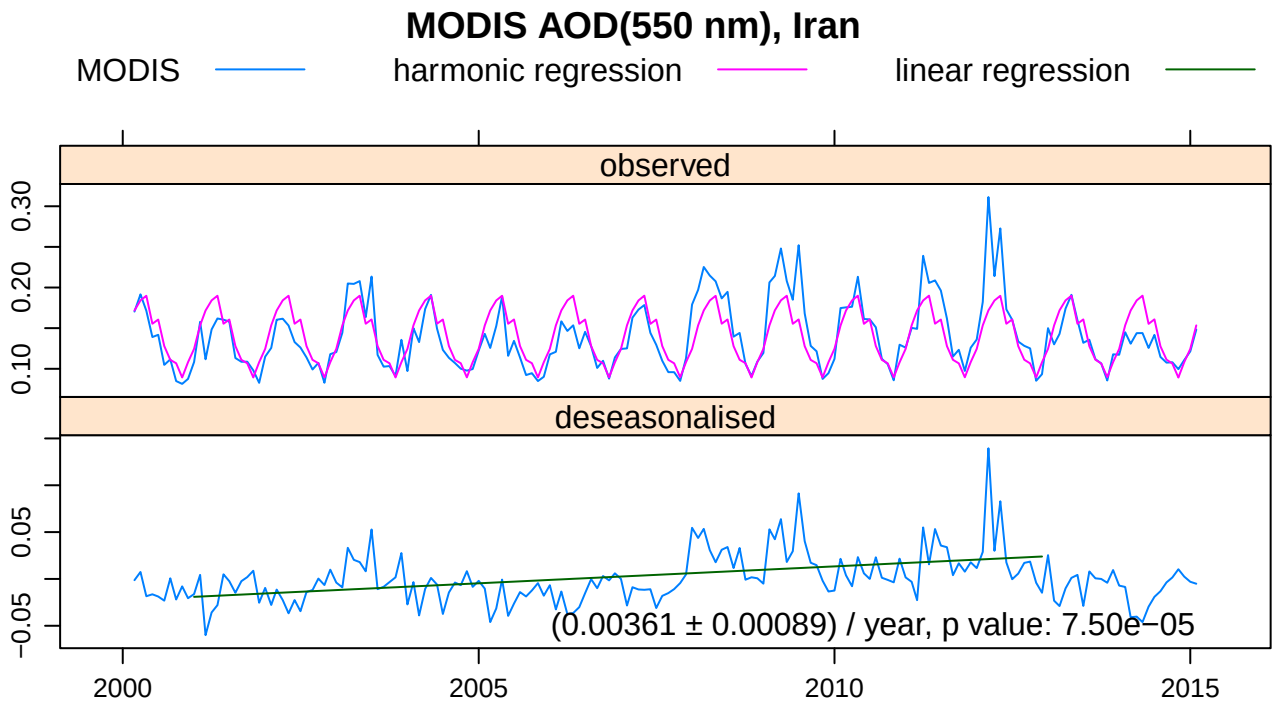

Figure S7. Same as Fig. 3, but for Iran.

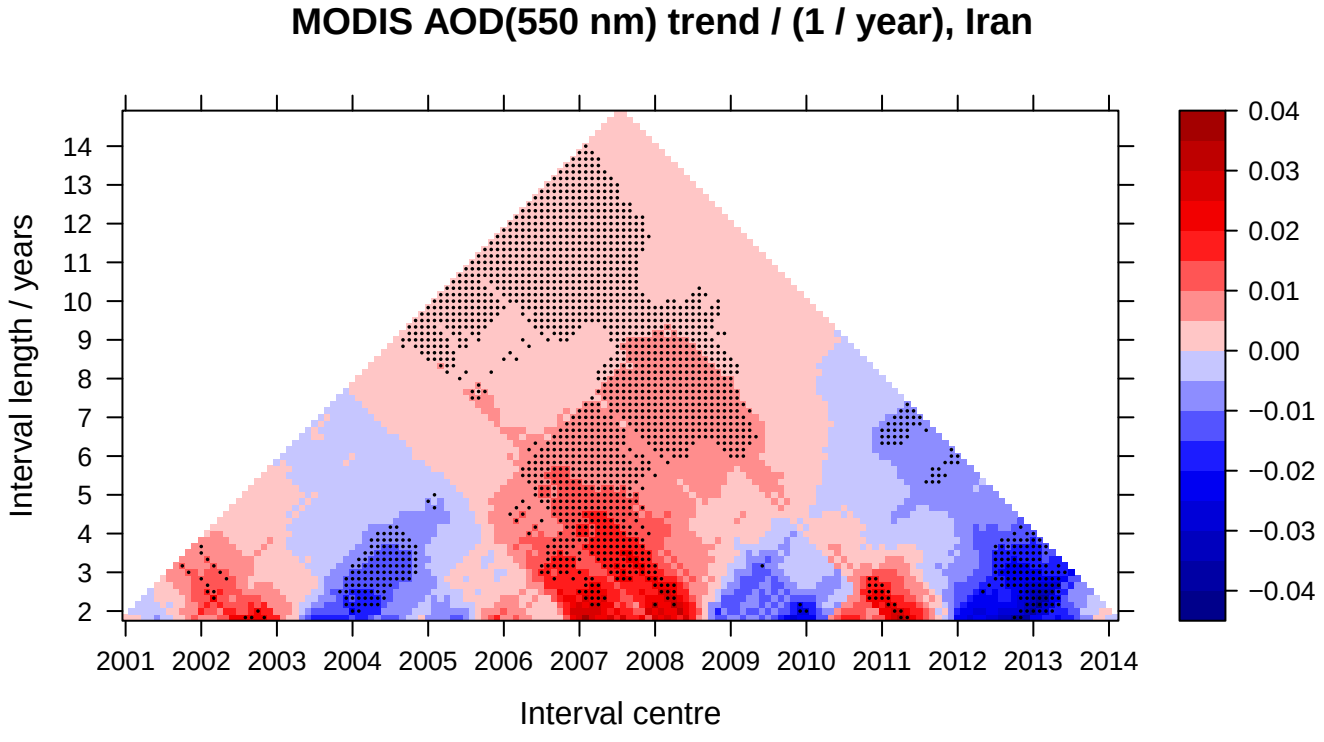

Figure S8. Same as Fig. S4, but for Iran.

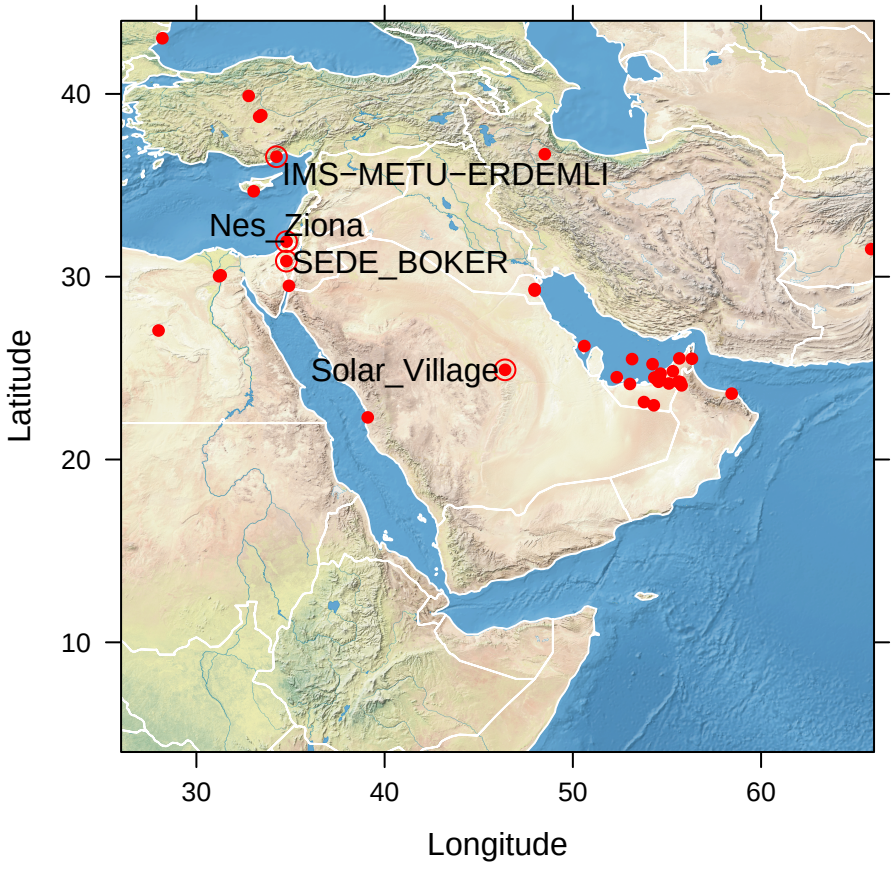

Figure S9. AERONET stations (red dots) in the region of interest. Stations with records extending over more than ten years of the current millennium are encircled and labelled.

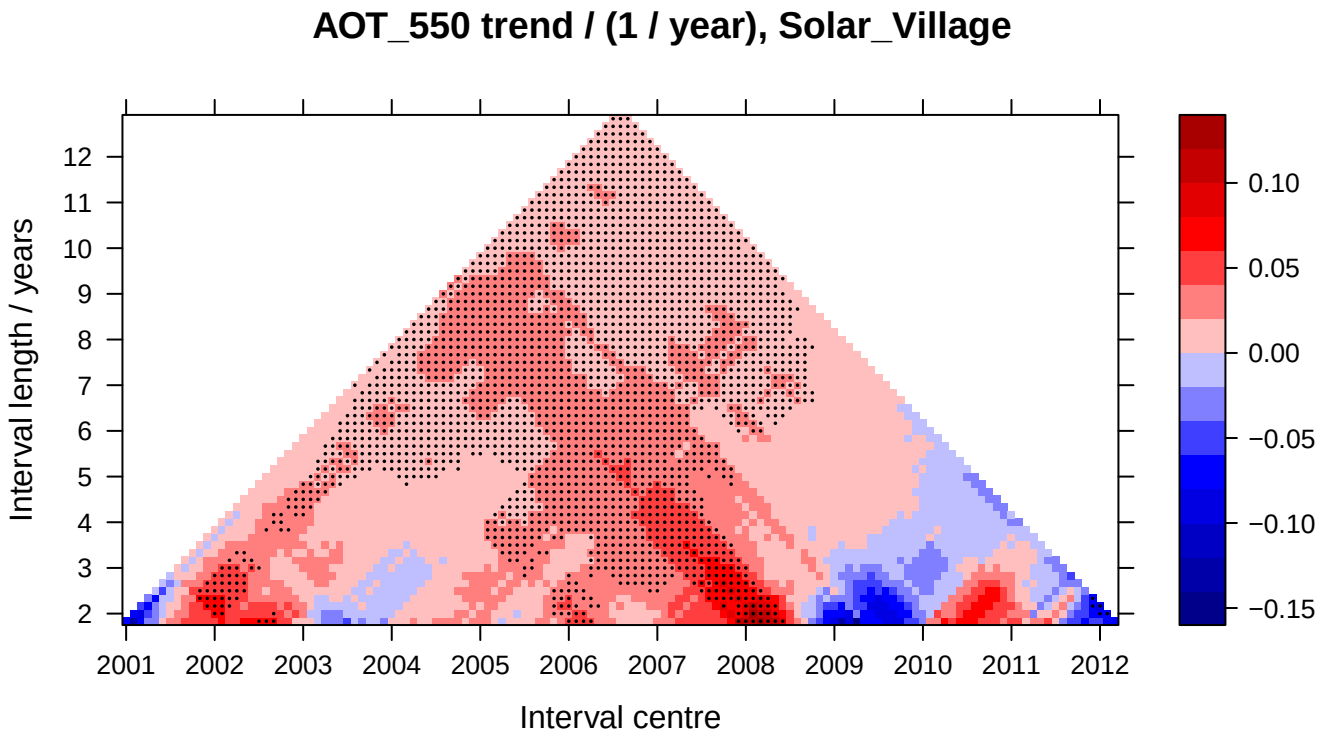

Figure S10. Same as Fig. S4, but for the AOD measured by the AERONET station *Solar Village*, linearly interpolated to 550 nm.

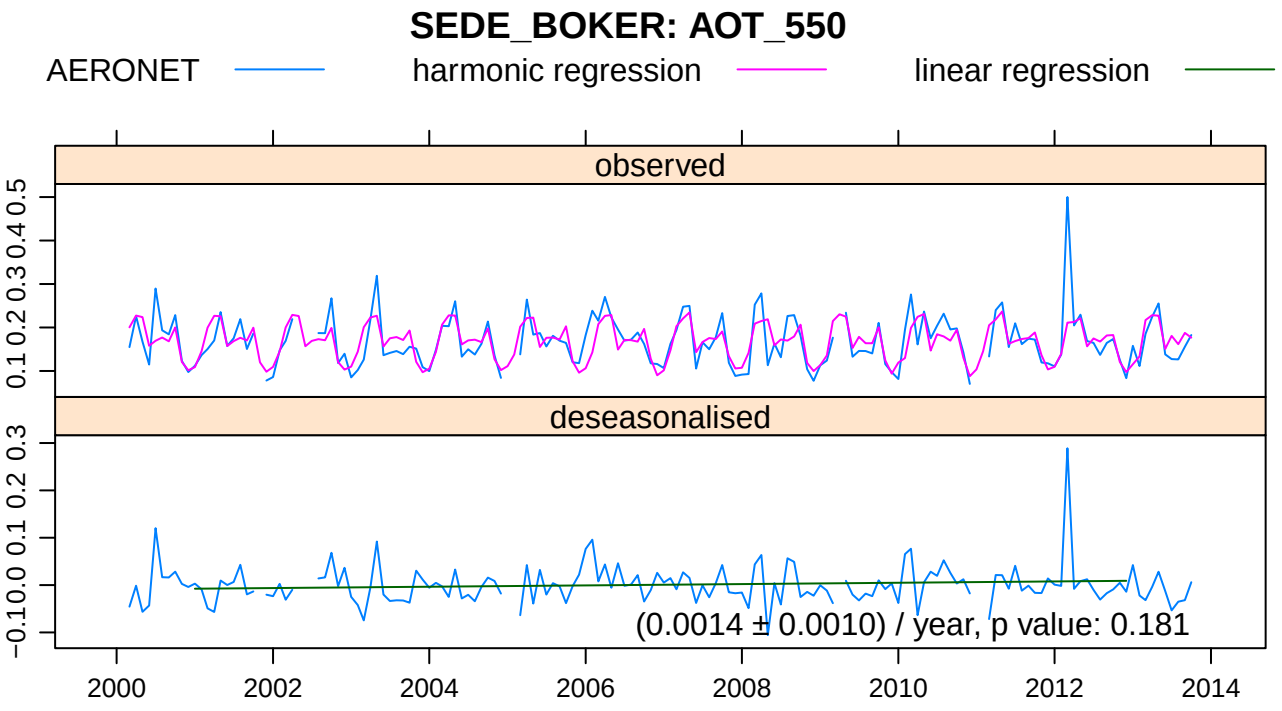

Figure S11. Same as Fig. 4, but for the AERONET station *SEDE BOKER*.

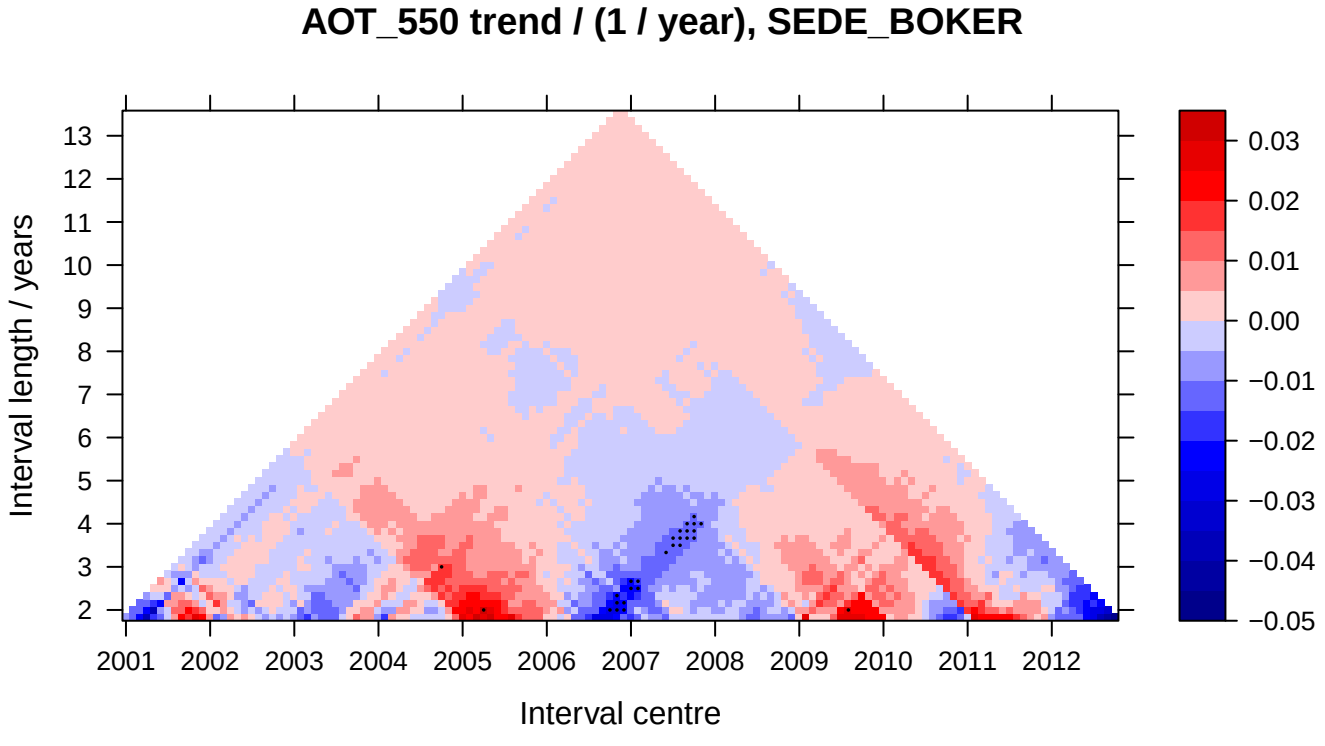

Figure S12. Same as Fig. S10, but for the AERONET station *SEDE BOKER*.

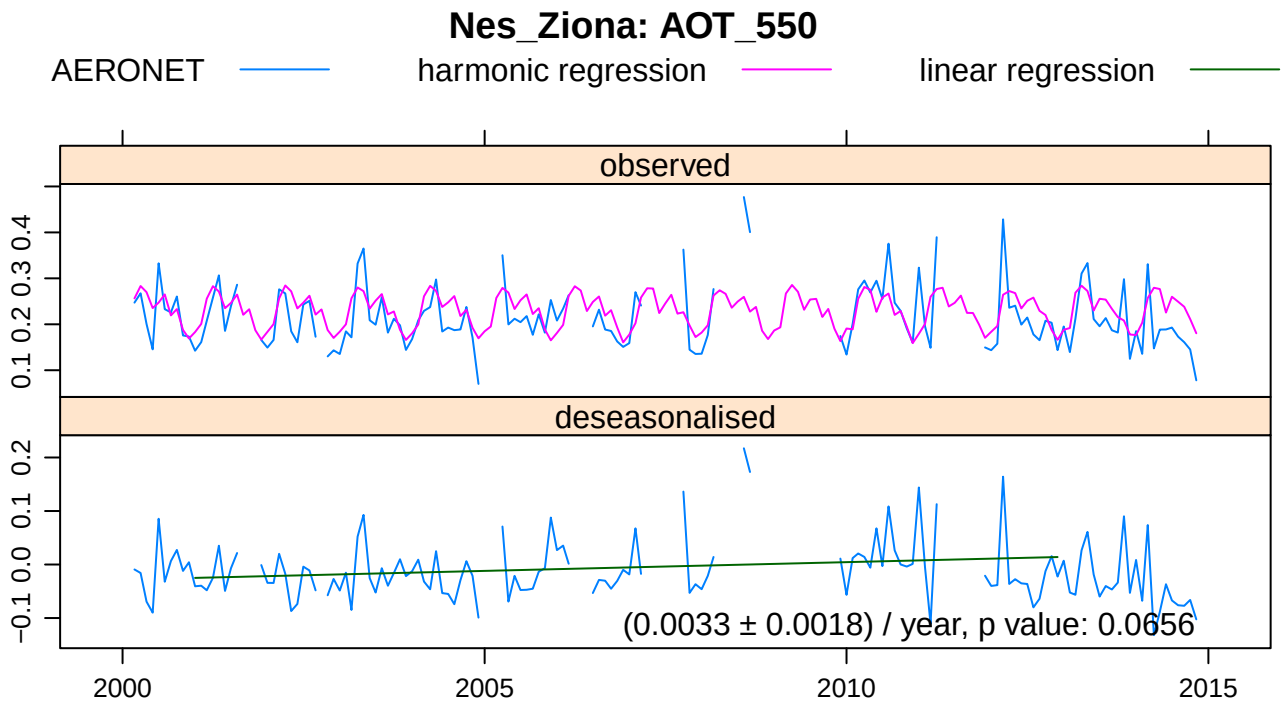

Figure S13. Same as Fig. 4, but for the AERONET station *Nes Ziona*.

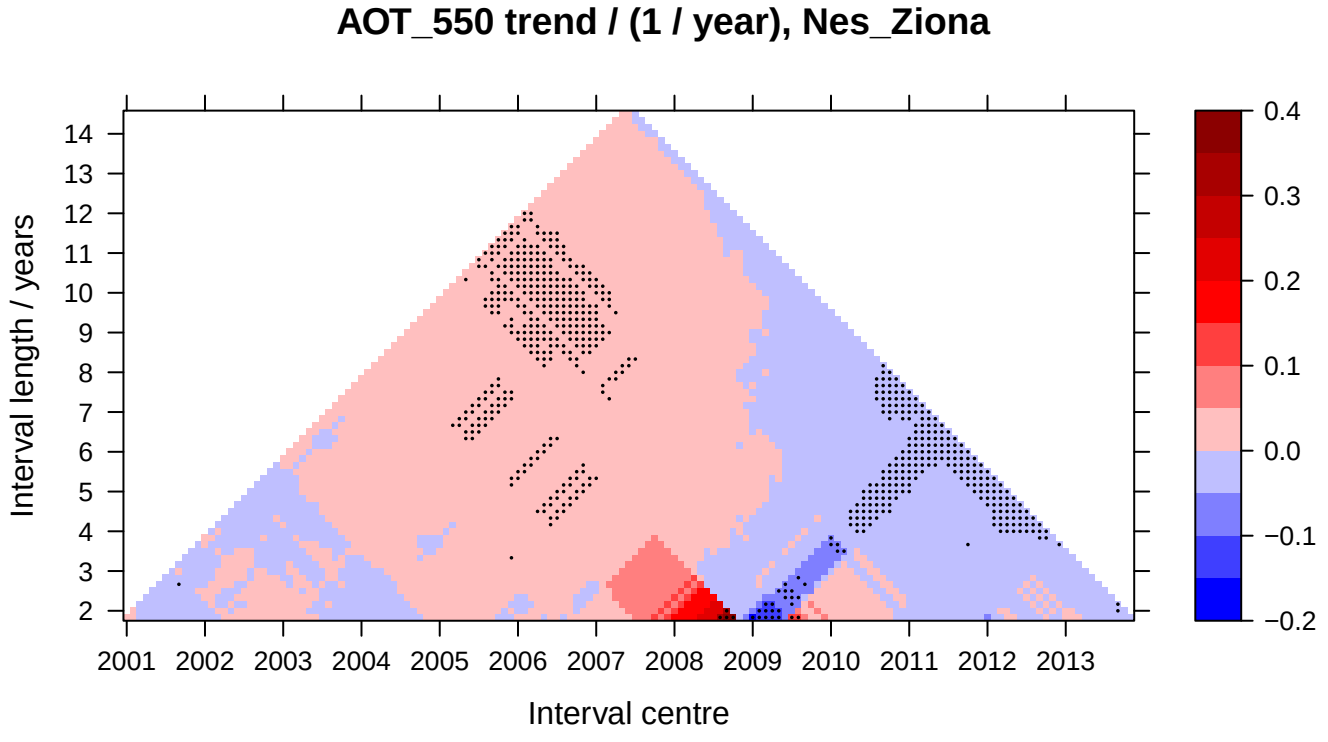

Figure S14. Same as Fig. S10, but for the AERONET station *Nes Ziona*.

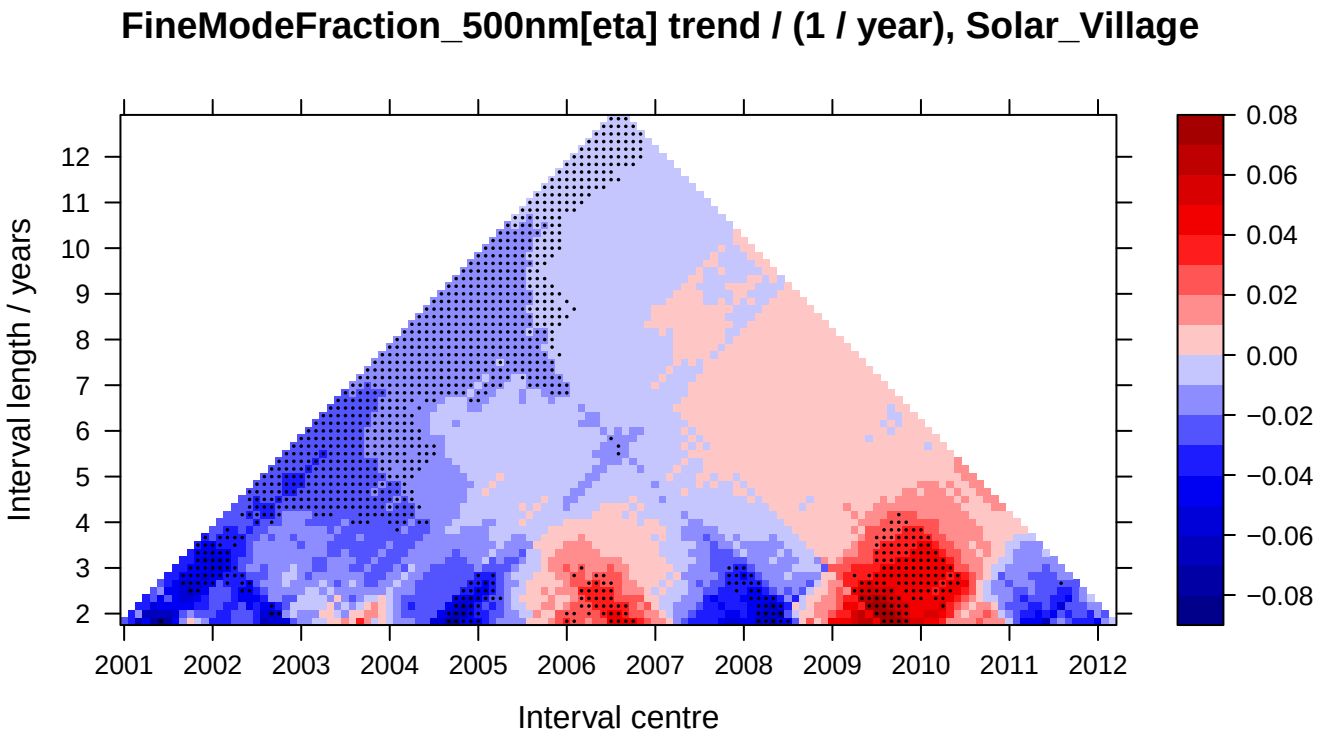

Figure S15. Same as Fig. S10 but for the AERONET fine mode fraction instead of the AOD.

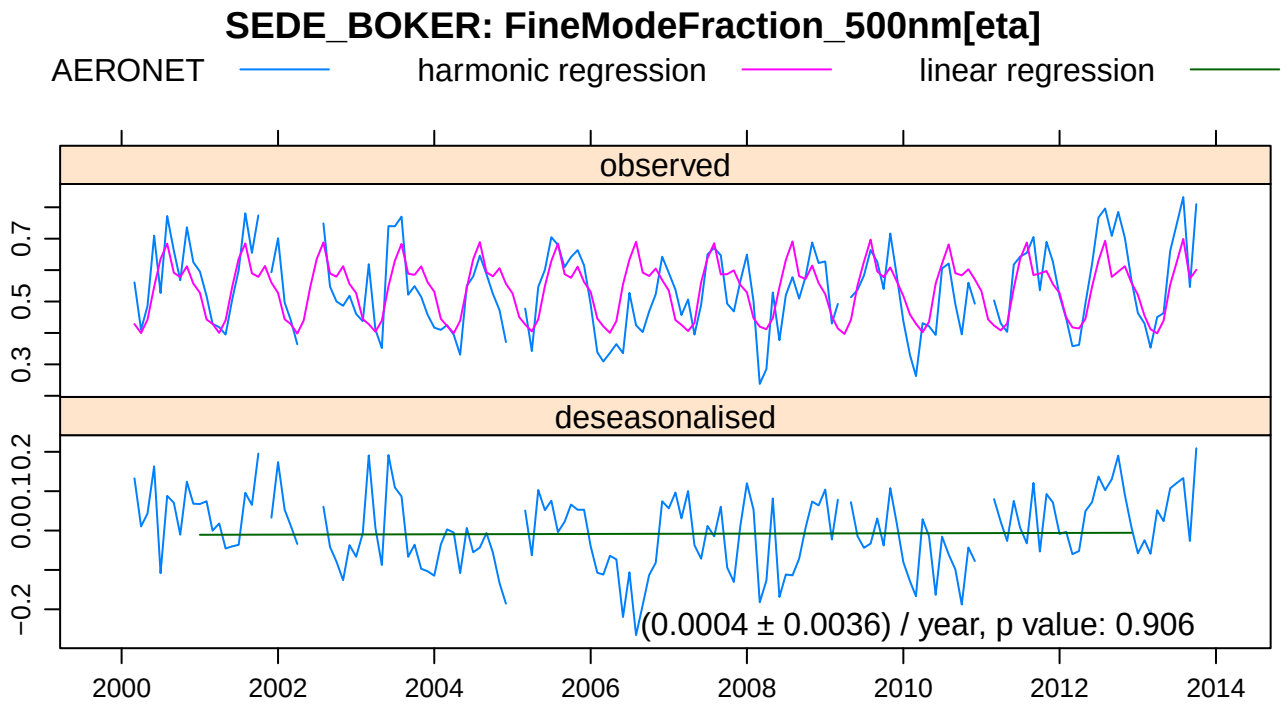

Figure S16. Same as Fig. 6 but for the AERONET station *SEDE BOKER*.

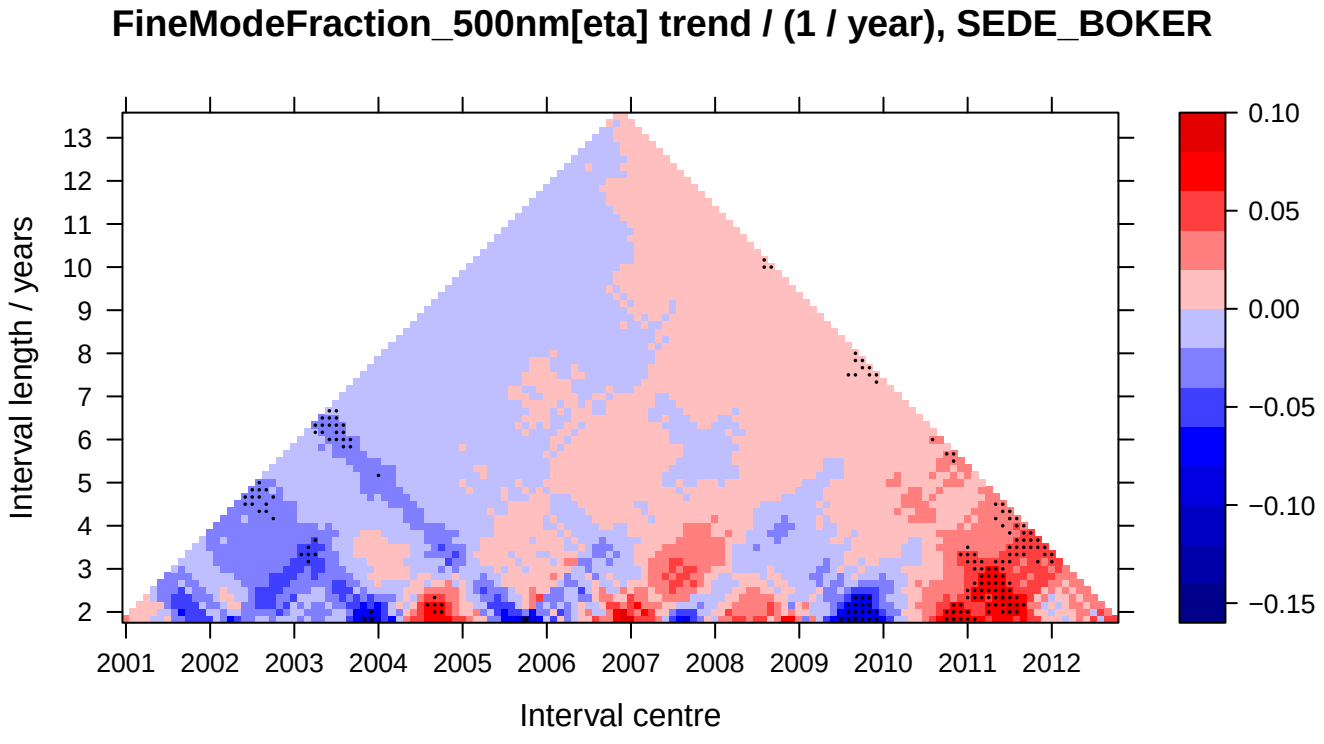

Figure S17. Same as Fig. S15 but for the AERONET station *SEDE BOKER*.

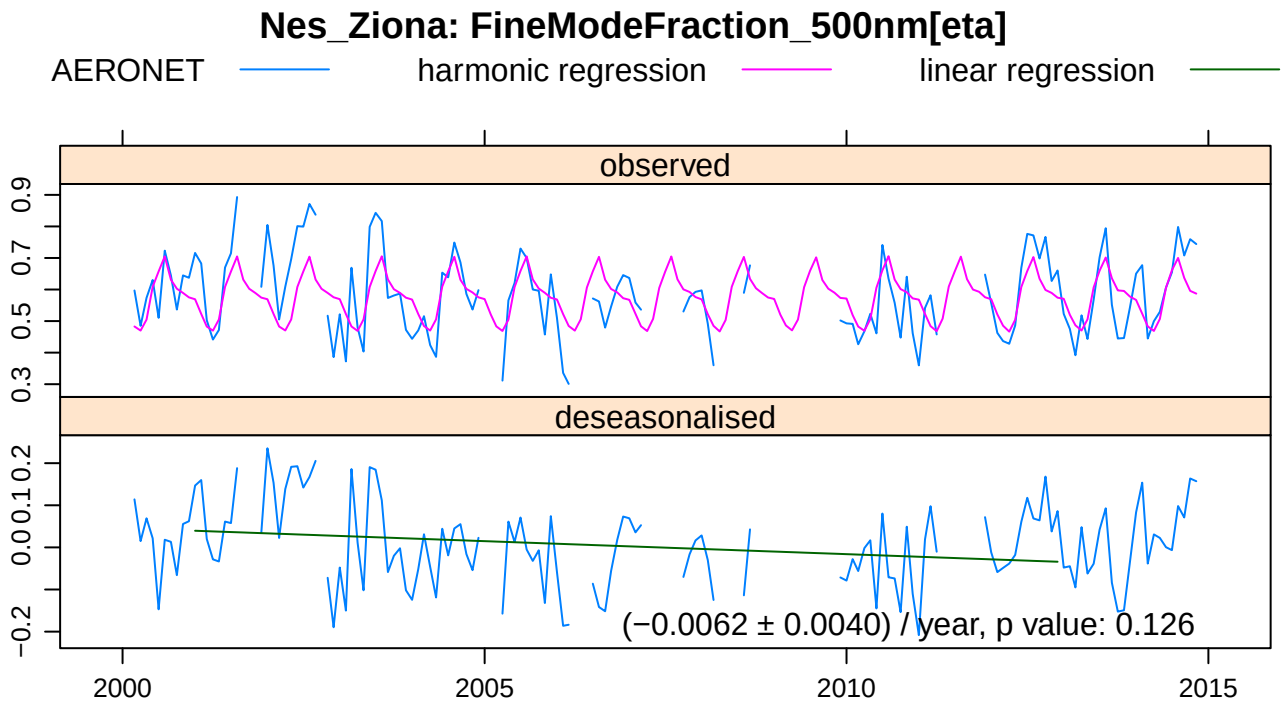

Figure S18. Same as Fig. 6 but for the AERONET station *Nes Ziona*.

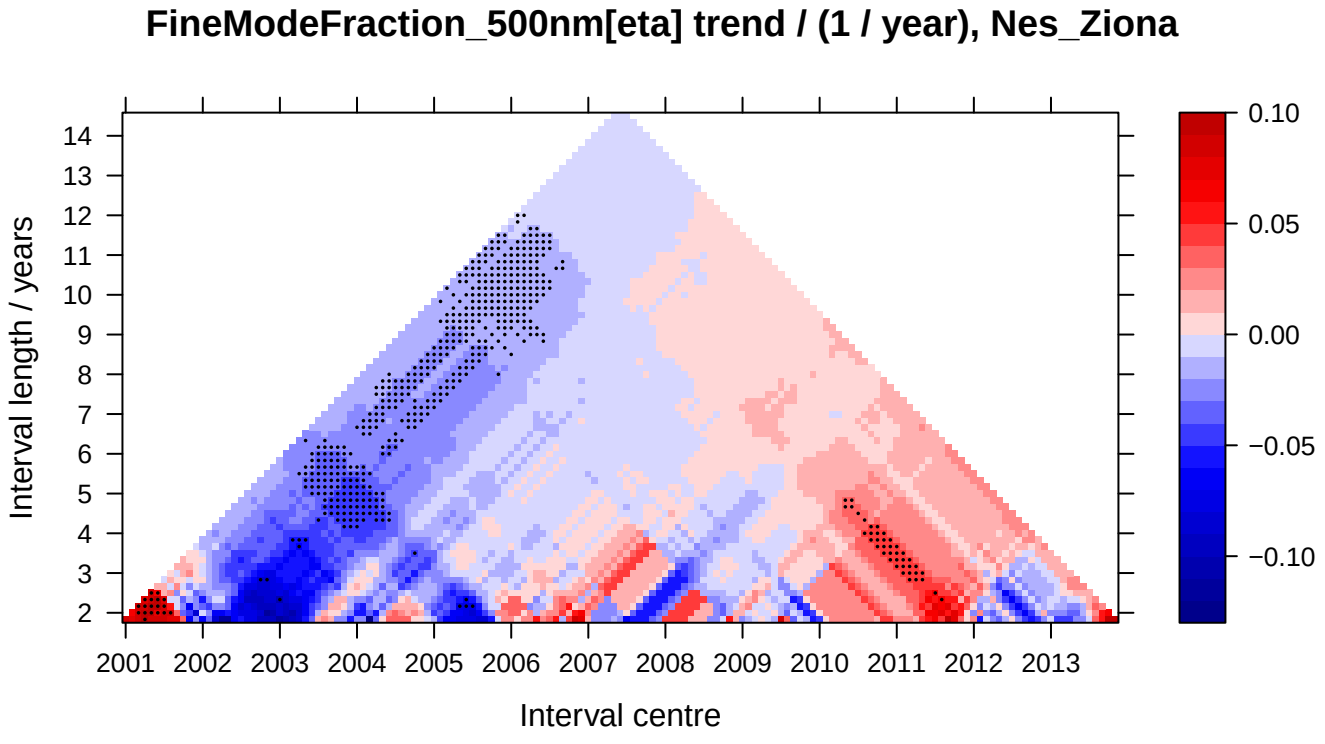

Figure S19. Same as Fig. S15 but for the station *Nes Ziona*.

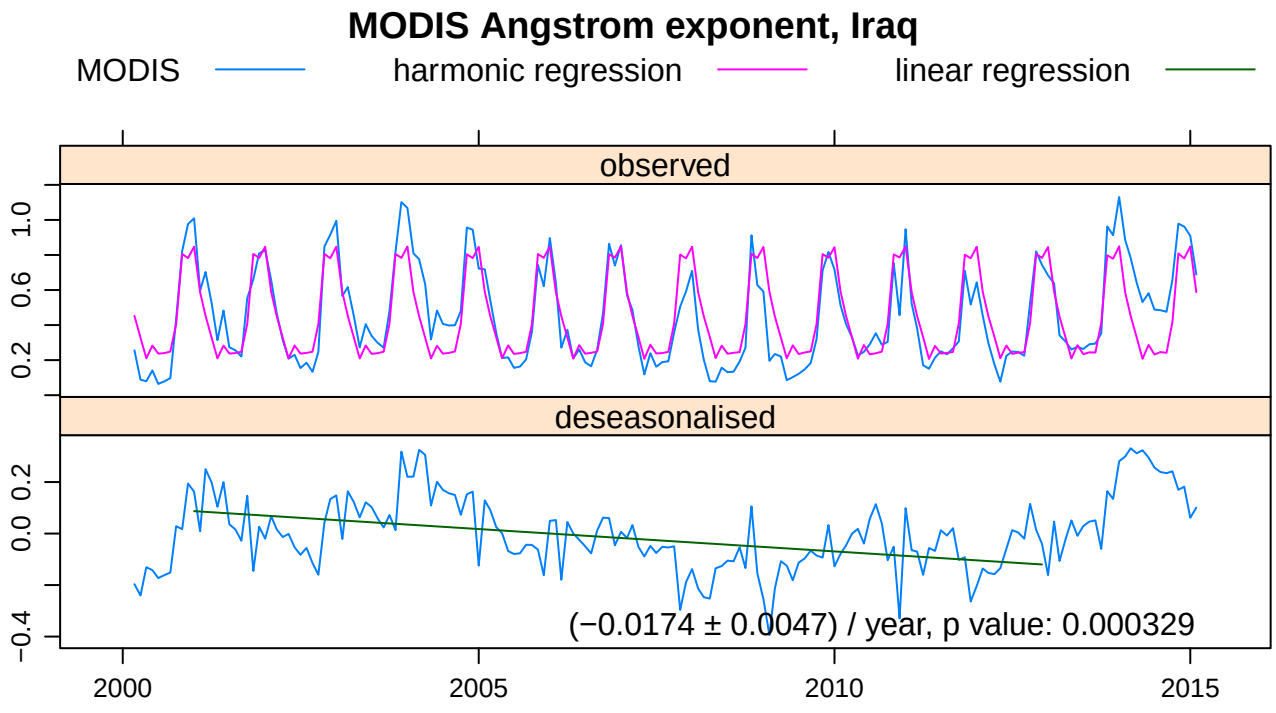

Figure S20. Same as Fig. 5, but for Iraq.

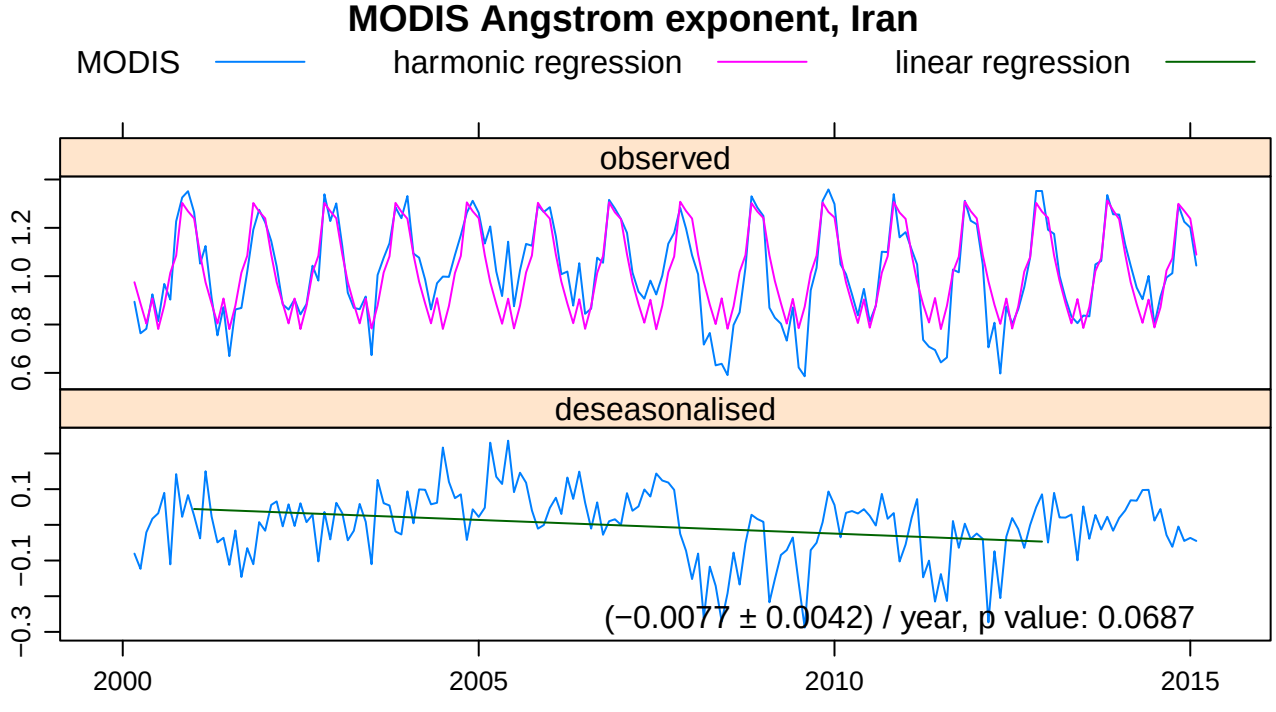

Figure S21. Same as Fig. 5, but for Iran.

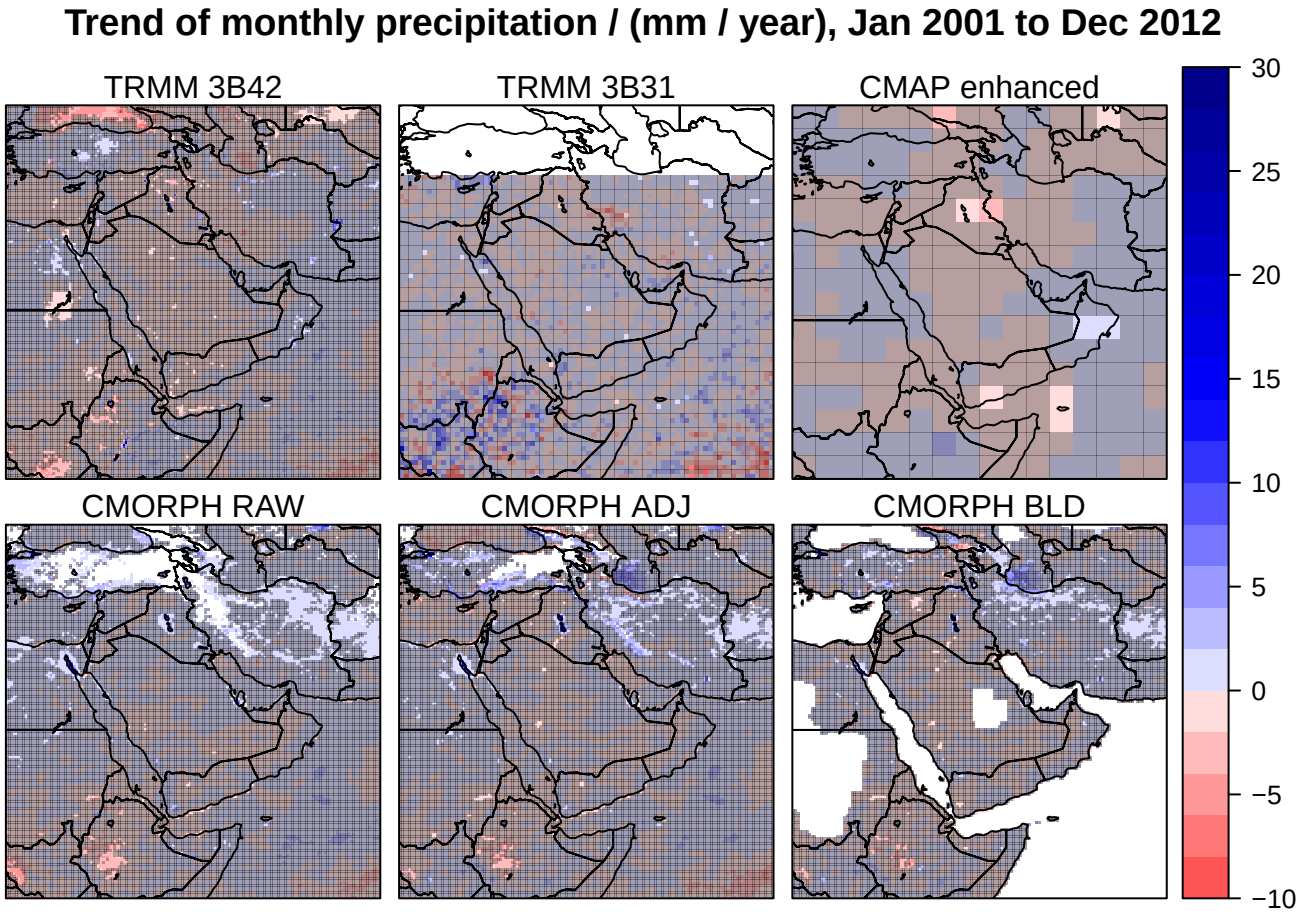

Figure S22. Pattern of Middle Eastern precipitation trends. Based on TRMM 3B42 daily, TRMM 3B31 monthly, CMAP enhanced monthly, CMORPH RAW daily, CMORPH ADJ daily and CMORPH BLD daily data, respectively. Pixels with non-significant trend (p value > 0.01) are shaded grey. See also Fig. S23.

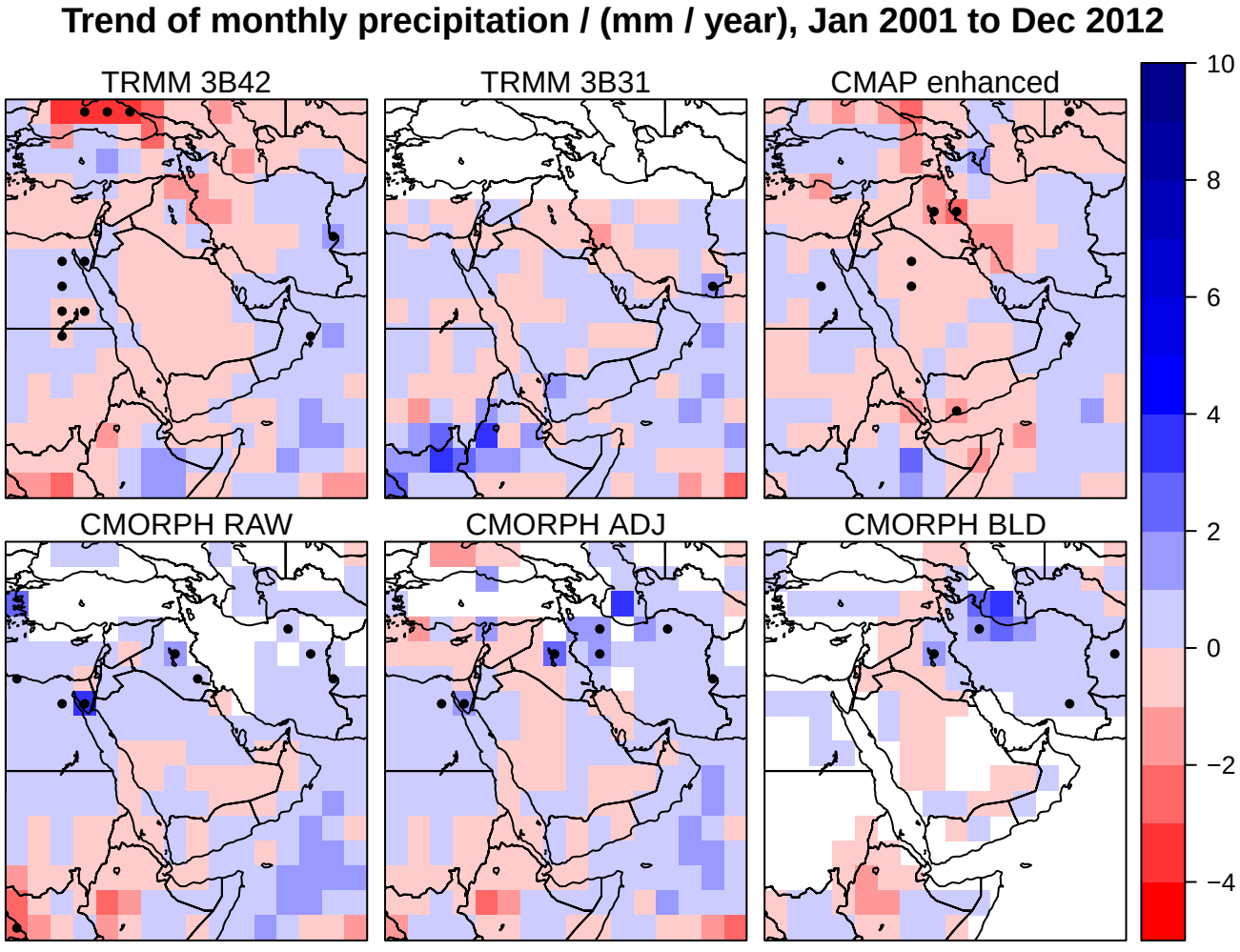

Figure S23. Pattern of Middle Eastern precipitation trends. Based on TRMM 3B42 daily, TRMM 3B31 monthly, CMAP enhanced monthly, CMORPH RAW daily, CMORPH ADJ daily and CMORPH BLD daily data, respectively. Pixels with significant trend (p value < 0.01) are marked with a dot. For better readability and to reduce statistical noise, all data sets have been re-gridded to the coarse 2.5° grid of the CMAP data (averaging over sub-pixels). Unlike for Fig. S22, annual averaged instead of deseasonalised values have been used to the compute trend, which can be more reliable in regions of very sporadic precipitation.

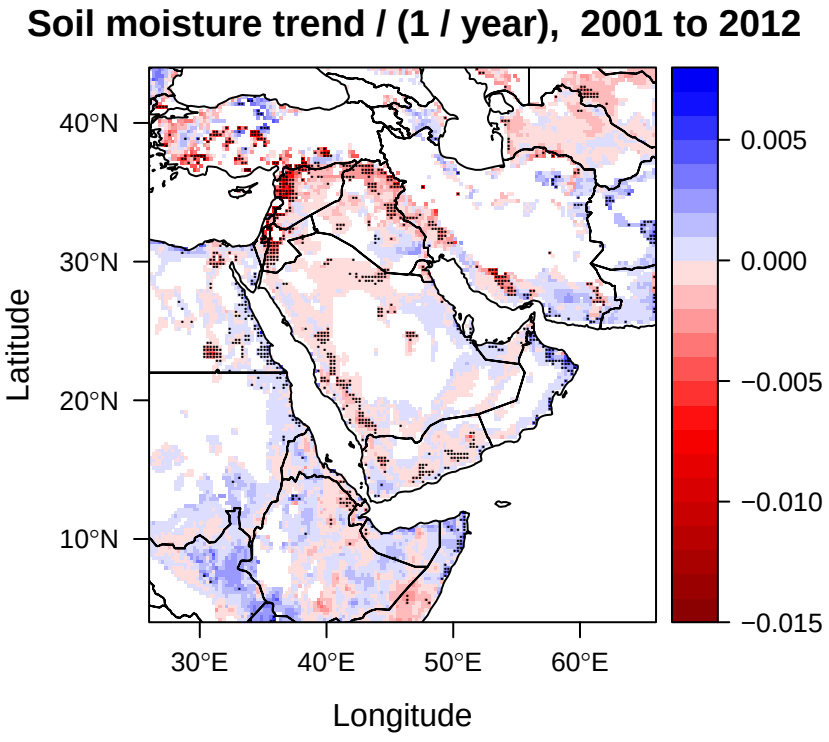

Figure S24. Pattern of Middle Eastern twelve year soil moisture trends for the twelve year period January 2001 to December 2012. Negative trends are even more pronounced when considering only the first ten years until 2010, see Fig. S25. Based on surface soil moisture (SSM) data from the European Space Agency Climate Change Initiative (ESA-CCI).

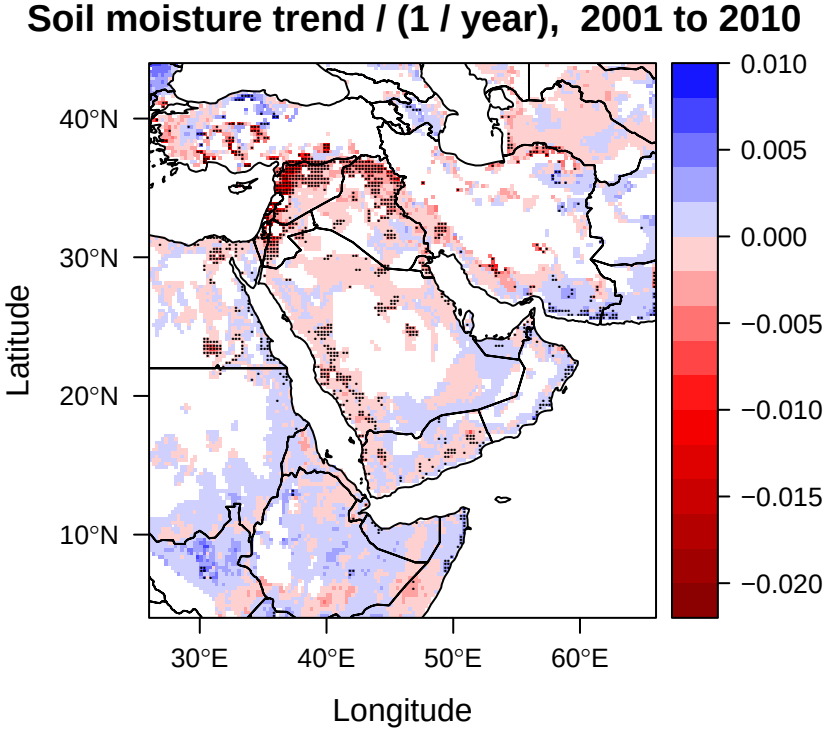

Figure S25. Same as Fig. S24 but for the time period 2001 to 2010.

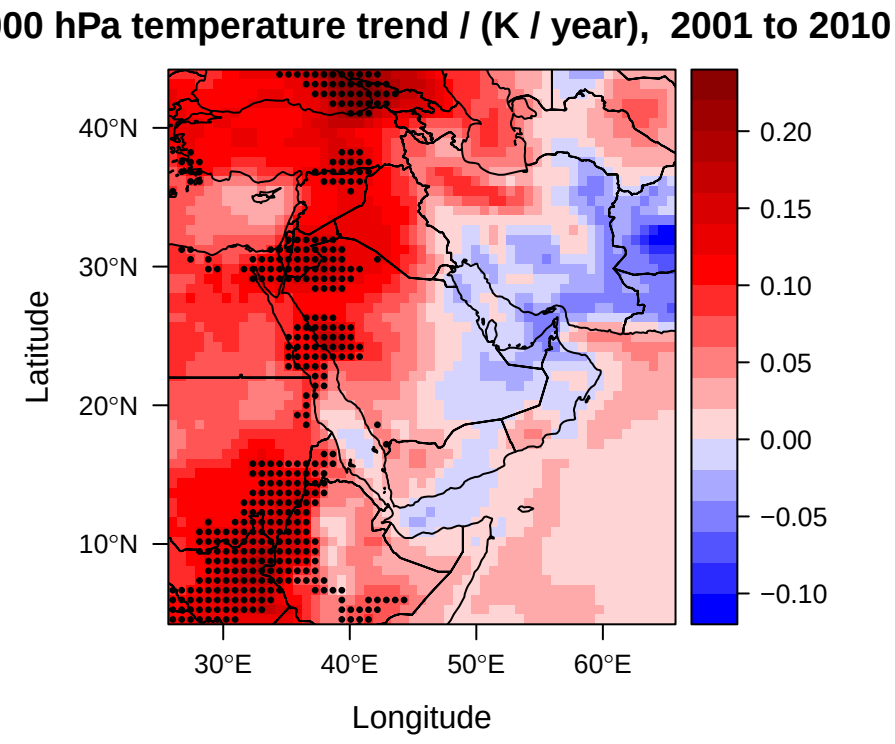

Figure S26. Pattern of Middle Eastern temperature trends (January 2001 to December 2010). The significant positive trend in several regions is interrupted by moderate temperatures in 2011, possibly slowing down the negative soil moisture trend (cp. S24 vs. S25). Based on the ERA-Interim 1000 hPa temperature.

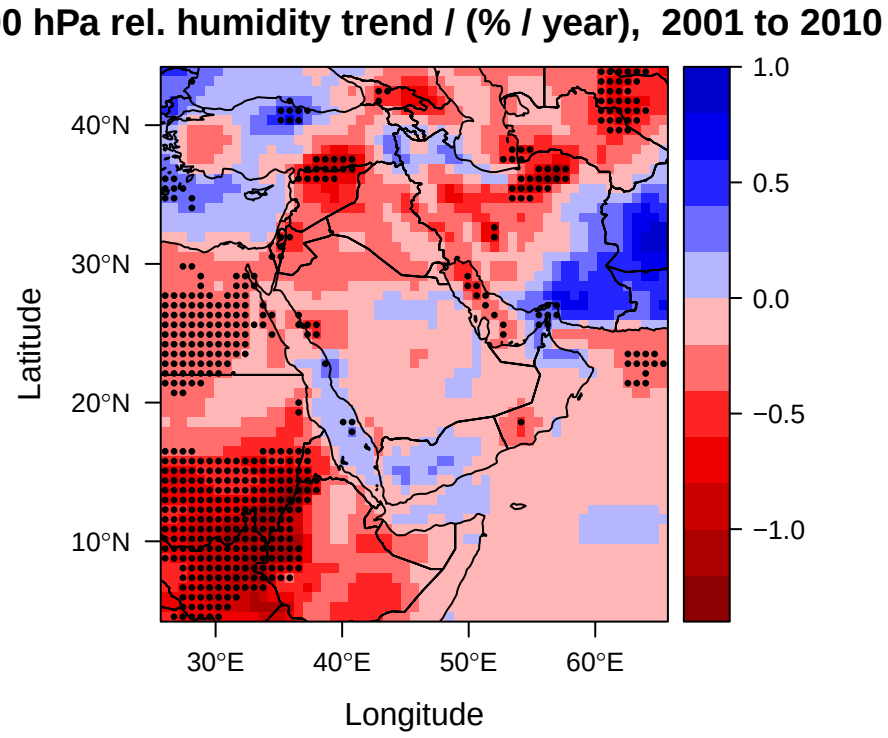

Figure S27. Pattern of Middle Eastern relative humidity trends (January 2001 to December 2010). Based on the ERA-Interim 1000 hPa relative humidity.

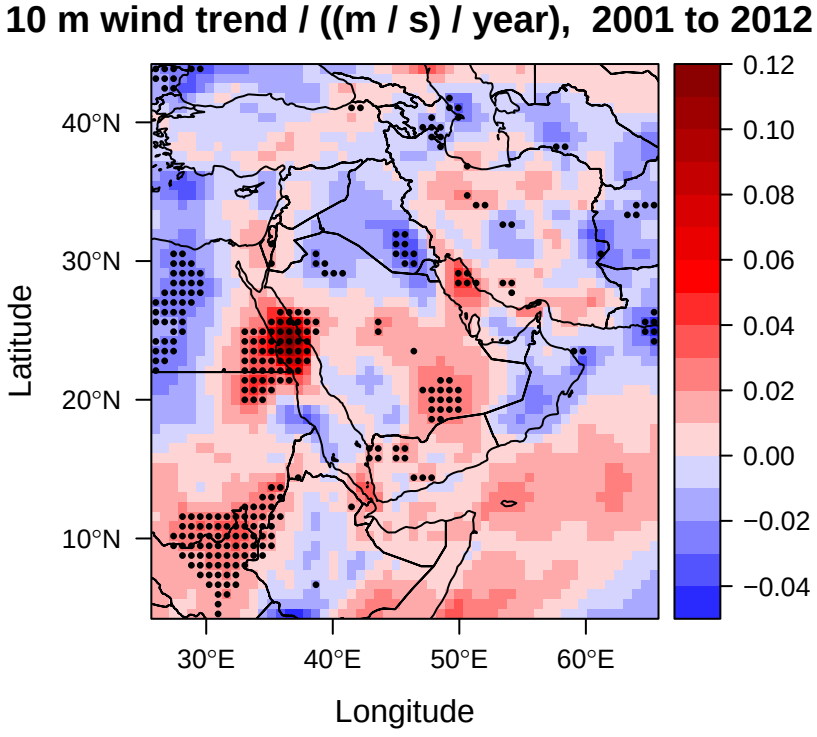

Figure S28. Pattern of Middle Eastern surface wind trends. Based on ERA-Interim wind at 10 m altitude.

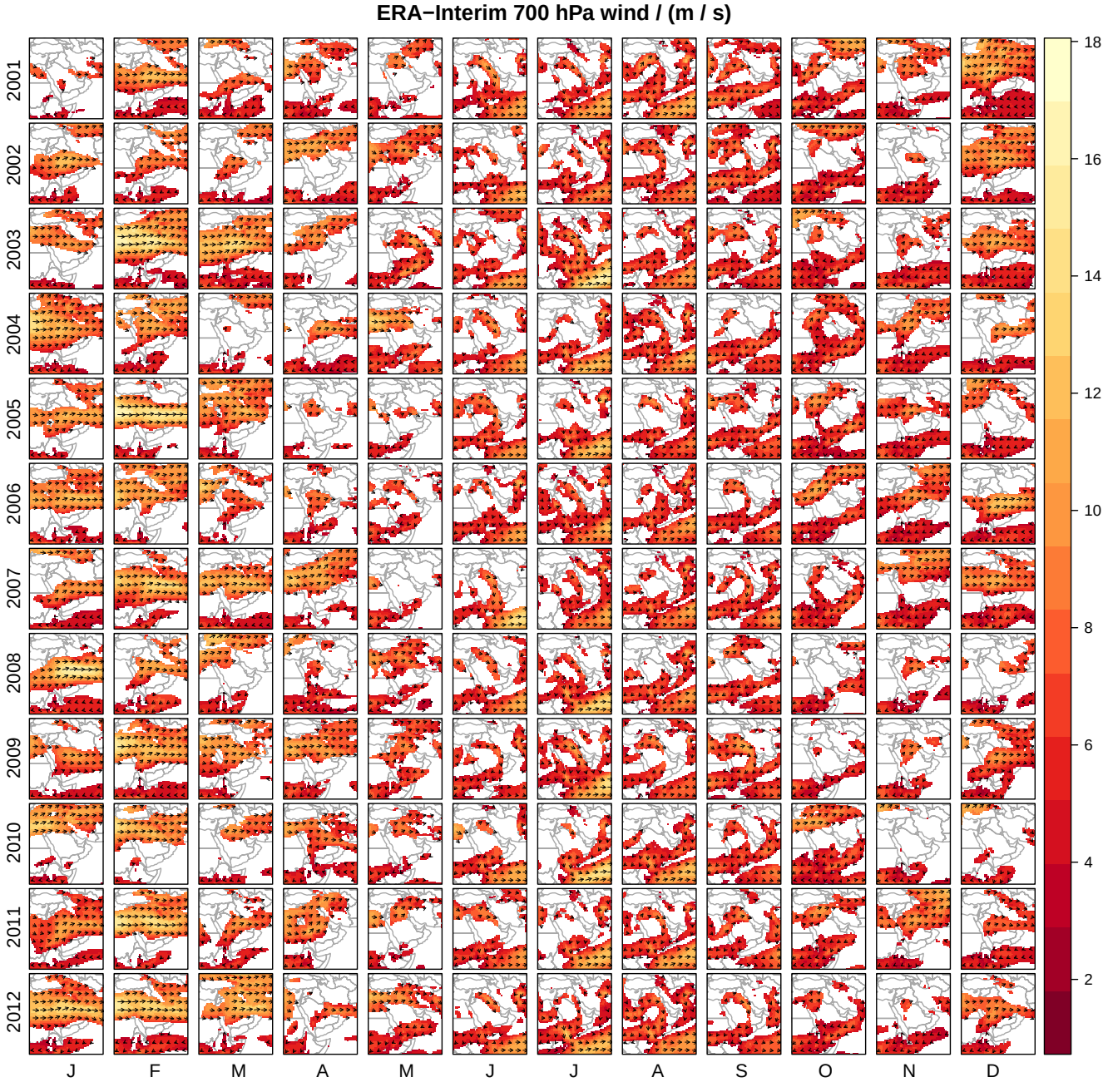

Figure S29. ERA-Interim wind at 700 hPa. To expose persistent transport patterns, monthly average wind vectors $(\bar{u}, \bar{v})^T$ are plotted if their magnitude exceeds $\sqrt{\sigma(u)^2 + \sigma(v)^2}$, where σ denotes the standard deviation of the six-hourly values. The colour scale reflects the vector magnitude.

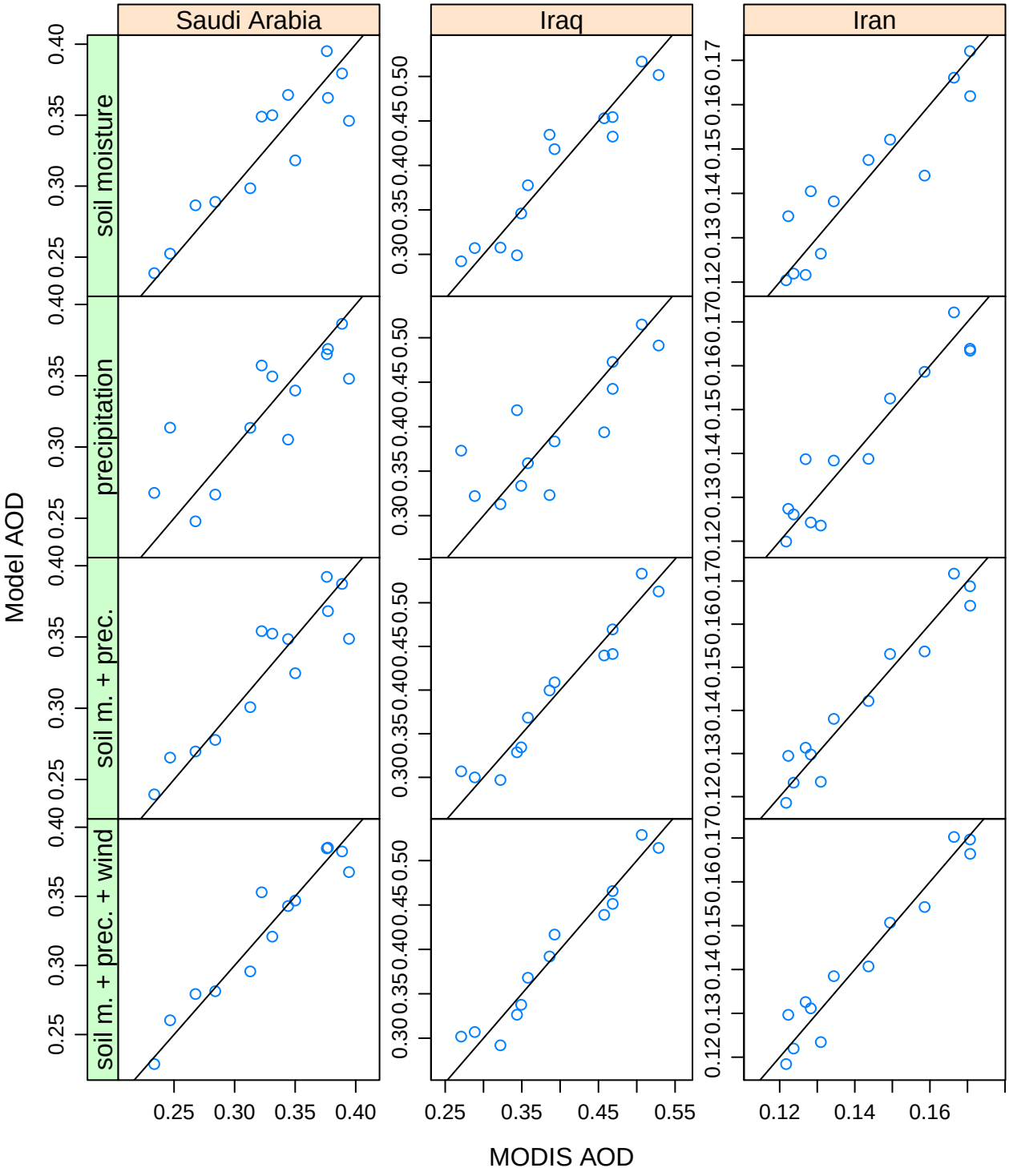

Figure S30. Linear model vs. MODIS AOD for the models in Tab. 1. The model predictors used in each row are displayed in the strip on the left. For Iraq and Iran, good model results are obtained when using soil moisture and precipitation as predictors (third row). For Saudi Arabia, the model can be improved by additionally considering the surface wind (bottom left).